Numerical determination of monopole entropy in pure SU(2) QCD

M. N. Chernodub,[1,2] Katsuya Ishiguro,[1] Katsuya Kobayashi,[1] and Tsuneo Suzuki[1]
[1]*Institute for Theoretical Physics, Kanazawa University, Kanazawa 920-1192, Japan*
[2]*Institute of Theoretical and Experimental Physics, B. Cheremushkinskaja 25, Moscow 117259, Russia*
(Received 5 June 2003; published 30 January 2004)

We study numerically the length distributions of the infrared monopole clusters in pure SU(2) QCD. These distributions are Gaussian for all studied blocking steps of monopoles, lattice volumes and lattice coupling constant. We also investigate the monopole action for the infrared monopole clusters. The knowledge of both the length distribution and the monopole action allows us to determine the effective entropy of the monopole currents. The entropy is a descending function of blocking scale, indicating that the effective degrees of freedom of the extended monopoles are getting smaller as the blocking scale increases.

DOI: 10.1103/PhysRevD.69.014509 PACS number(s): 11.15.Ha, 12.38.Gc, 14.80.Hv

I. INTRODUCTION

The dual superconductor picture [1] of the QCD vacuum is one of the most promising approaches to the problem of color confinement. This picture is based on the existence of Abelian monopoles in the vacuum of QCD. The monopoles are identified with the help of the Abelian projection method [2], which is based on a partial gauge fixing of the SU(N) gauge symmetry up to an Abelian subgroup. The monopoles naturally appear in the Abelian projection due to compactness of the residual Abelian group.

There are various numerical indications that the monopoles are responsible for the confinement of quarks (for a review, see Ref. [3]). One of the most important observations is the monopole condensation in the low temperature (confinement) phase [4,5]. According to the dual superconductor mechanism the monopole condensation gives rise to the formation of the chromoelectric string which confines the fundamental color sources. This expectation is confirmed by the fact that the nonzero tension of the chromoelectric string is dominated by the Abelian monopole contributions [6–8].

In the numerical simulations one observes that the trajectories of the Abelian monopoles form clusters, which can be divided into two ensembles: finite-sized clusters and one large percolating cluster [9–11]. The percolating cluster [or infrared (IF) cluster] occupies the whole lattice while the finite-sized clusters have an ultraviolet (UV) nature. The existence of the IR cluster is related to the monopole condensation [9]. The importance of the IR cluster for the confinement of quarks was also stressed in numerical calculations [10]: the tension of the confining string gets a dominant contribution from the monopoles belonging to the IR cluster, while the contribution of the UV clusters to the string tension is negligible. The IR cluster disappears in the deconfinement phase [9,10], as expected.

The balance between energy and entropy of the elementary monopole trajectories plays an important role. For example, the compact U(1) gauge model in four dimensions has a phase transition associated with the monopole condensation. Actually the phase transition occurs at the point on the phase diagram where the entropy and the energy of the monopole trajectories are the same. The authors of Ref. [22] found the critical value of the U(1) gauge coupling constant with a great accuracy using the fact. The energy-entropy balance was also studied numerically for the monopoles in compact U(1) gauge theory [23] and in finite-temperature pure SU(2) gauge theory [10].

In this paper we mostly concentrate on the numerical investigation of the properties of the infrared monopole cluster. The length distributions and other properties of the UV and the IR clusters were studied previously in Refs. [10–14,18]. In this publication we investigate thoroughly the properties of the length distributions of the monopole clusters for various lattice volumes and sizes of the extended monopoles.

The plan of the paper is the following. In Sec. II we describe the model and provide the details of numerical simulations. Section III is devoted to the investigation of the Abelian monopole action obtained by an inverse Monte Carlo method. The distribution of the cluster length in the infrared clusters is studied in Sec. IV. The knowledge of the monopole action and cluster distribution allows us, for the first time, to calculate the entropy of the lattice monopoles of various sizes. Our conclusions are presented in the last section.

II. MODEL AND SIMULATION DETAILS

We study the pure SU(2) gluodynamics with the lattice Wilson action, $S(U)=-(\beta/2)\mathrm{Tr}\,U_P$, where β is the coupling constant and U_P is the SU(2) plaquette constructed from the link fields. All our results are obtained in the maximal Abelian (MA) gauge [15] which is defined by the maximization of a lattice functional

$$R=\sum_{s,\hat{\mu}}\mathrm{Tr}(\sigma_3\tilde{U}(s,\mu)\sigma_3\tilde{U}^{\dagger}(s,\mu)), \tag{1}$$

with respect to gauge transformations $U(s,\mu)\to\tilde{U}(s,\mu)=\Omega(s)U(s,\mu)\Omega^{\dagger}(s+\hat{\mu})$. The local condition of maximization can be written in the continuum limit as the differential equation $(\partial_\mu+igA^3_\mu)(A^1_\mu-iA^2_\mu)=0$. Both this condition and the functional (1) are invariant under residual U(1) gauge transformations, $\Omega^{\mathrm{Abel}}(\omega)=\mathrm{diag}(e^{i\omega(s)},e^{-i\omega(s)})$.

The next step is Abelian projection of non-Abelian link variables to the Abelian ones after the gauge fixing is done. An Abelian gauge field is extracted from the $SU(2)$ link variables as follows:

$$\tilde{U}(s,\mu)=\begin{pmatrix} [1-|c(s,\mu)|^2]^{1/2} & -c^*(s,\mu) \\ c(s,\mu) & [1-|c(s,\mu)|^2]^{1/2} \end{pmatrix} \times \begin{pmatrix} u(s,\mu) & 0 \\ 0 & u^*(s,\mu) \end{pmatrix}, \quad (2)$$

where $u(s,\mu)=\exp(i\theta(s,\mu))$ represents the Abelian link field and $c(s,\mu)$ corresponds to charged matter fields.

The Abelian field strength $\theta_{\mu\nu}(s)\in(-4\pi,4\pi)$ is defined on lattice plaquettes by a link angle $\theta(s,\mu)\in[-\pi,\pi)$ as $\theta_{\mu\nu}(s)=\theta(s,\mu)+\theta(s+\hat{\mu},\nu)-\theta(s+\hat{\nu},\mu)-\theta(s,\nu)$. The field strength $\theta_{\mu\nu}(s)$ can be decomposed into two parts,

$$\theta_{\mu\nu}(s)=\overline{\theta}_{\mu\nu}(s)+2\pi m_{\mu\nu}(s), \quad (3)$$

where $\overline{\theta}_{\mu\nu}(s)\in[-\pi,\pi)$ is interpreted as the electromagnetic flux through the plaquette and $m_{\mu\nu}(s)$ can be regarded as a number of the Dirac strings piercing the plaquette.

The elementary monopole current is conventionally constructed using the DeGrand-Toussaint [16] definition:

$$k_\mu(s)=\frac{1}{2}\epsilon_{\mu\nu\rho\sigma}\partial_\nu m_{\rho\sigma}(s+\hat{\mu}), \quad (4)$$

where ∂ is the forward lattice derivative. The monopole current is defined on a link of the dual lattice and takes values $0,\pm1,\pm2$. Moreover the monopole current satisfies the conservation law automatically,

$$\partial'_\mu k_\mu(s)=0, \quad (5)$$

where ∂' is the backward derivative on the dual lattice.

Besides the elementary monopoles one can also define extended monopoles [9]. In this paper we use the type-2 construction according to the classification of the extended monopoles adopted in Ref. [9]. The n^3 extended monopole is defined on a sublattice with the lattice spacing $b=na$, where a is the spacing of the original lattice. Thus the construction of the extended monopoles corresponds to a block spin transformation of the monopole currents with the scale factor n,

$$k^{(n)}_\mu(s)=\sum_{i,j,l=0}^{n-1} k_\mu[ns+(n-1)\hat{\mu}+i\hat{\nu}+j\hat{\rho}+l\hat{\sigma}]. \quad (6)$$

The Abelian dominance and the monopole dominance in the infrared region of QCD imply that at least important infrared observables (such as the fundamental string tension) can be calculated using the Abelian fields or the monopole degrees of freedom only.

In what follows we discuss an effective model of the monopole currents corresponding to pure SU(2) QCD. Formally, we get this effective model through the gauge fixing procedure applied to the original model. We integrate out all degrees of freedom but the monopole ones. An effective Abelian action is related to the original non-Abelian action $S[C,\theta]$ [matter C and Abelian gauge θ fields in Eq. (2)] as follows:

$$Z=\int \mathcal{D}u\left[\int DC e^{-S[C,\theta]}\delta(X)\Delta_{FP}(U)\right] = \int \mathcal{D}u e^{-S_{eff}[\theta]}. \quad (7)$$

Here and below we omit irrelevant constant terms in front of the partition functions. In Eq. (7) the term $\delta(X)$ represents the gauge-fixing condition[1] and $\Delta_{FP}(U)$ is the corresponding Faddeev-Popov determinant. Next step is to relate the effective U(1) action to the effective monopole action:

$$Z=\left(\prod_{s,\mu}\sum_{k_\mu(s)=-\infty}^{\infty}\right) \times\int \mathcal{D}\theta\,\delta(k_\mu(s)-k_\mu(s;\theta))e^{-S^{\rm Abel}_{\rm eff}[\theta]} \quad (8)$$

$$=\left(\prod_{s,\mu}\sum_{k_\mu(s)=-\infty}^{\infty}\right)\left(\prod_s \delta_{\partial'_\mu k_\mu(s),0}\right)e^{-S^{\rm mon}_{\rm eff}[k]}, \quad (9)$$

where $k_\mu(s;\theta)$ is the monopole current defined as a function of the Abelian fields θ as shown in Eqs. (3) and (4).

Our simulation statistics is represented in Table I. The gauge configurations were generated with the help of the standard Monte Carlo algorithm. In most simulations we use the usual iterative algorithm to fix the MA gauge. However, in order to check the Gribov copy dependence of the MA gauge fixing we also use the so called simulated annealing (SA) algorithm with five Gribov copies. We refer the reader for a detailed description of the SA method to Ref. [17], where the advantages of the SA method compared to the iterative algorithm are illustrated.

TABLE I. Simulation statistics.

Lattice size	β	Blocking factor	Number of configurations
6	2.1–2.4	1	3000
8	2.1–2.4	1	3000
10	2.1–2.4	1	3000
12	2.1–2.4	2	3000
14	2.1–2.4	1	3000
16	2.1–2.4	2	3000
24	2.1–2.4	2,3,4	3000
32(SA)	2.1–2.6	2,3	950
48	2.1–2.6	2,3,4,6,8	2200

[1]As we discussed above, the MA gauge fixing condition is given by the maximization of the functional (1) and therefore the use of the local condition $X=0$ in Eq. (7) is a formal simplified notation.

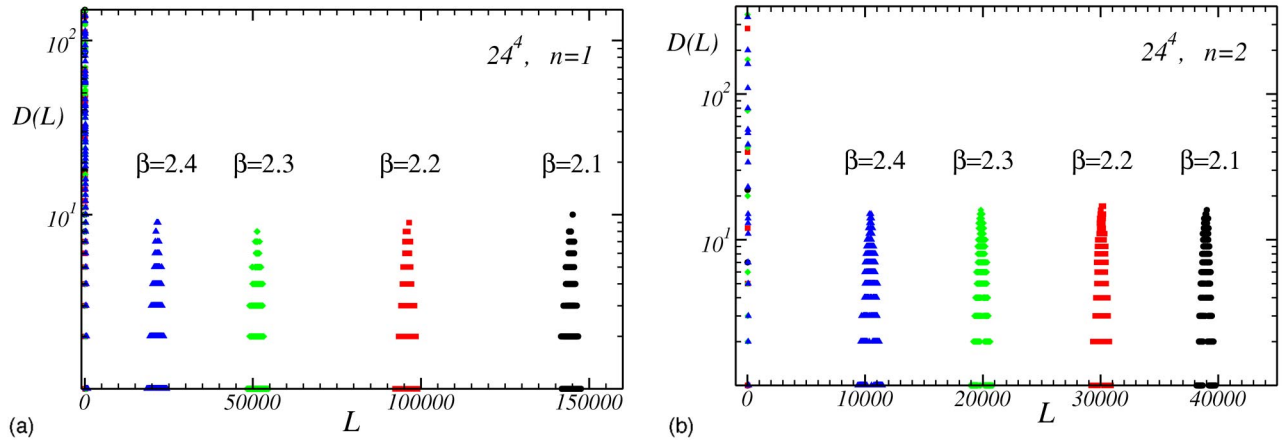

FIG. 1. Distribution of the lengths of the monopole trajectories at various β for (a) elementary and (b) $n=2$ blocked monopoles.

III. MONOPOLE ACTION FOR VARIOUS CLUSTERS

It is well known that monopole trajectories can be separated into the infrared and the ultraviolet monopole clusters in gluodynamics. Each configuration contains typically only one IR monopole cluster. This cluster occupies all volume of the lattice and the length of the IR monopole trajectory is proportional to the volume of the lattice. Besides the IR cluster each configuration contains also a large number of shorter monopole trajectories (UV clusters).

A simplest characteristics of the monopole trajectory is its length. Using a large enough number of the vacuum configurations, one can construct a distribution of the lengths $D(L)$ of the IR and the UV monopole clusters. The length distribution is a function of the length of the monopole trajectory which is equal to the number of clusters with the monopole length L found in the ensembles of the vacuum configurations.

In Fig. 1(a) we show typical distributions of the elementary ($n=1$) monopoles. The distribution at each value of the coupling constant β has two peaks corresponding to the UV monopole clusters (the peak at small L) and to the IR clusters (at large L). We plot the distributions calculated at various values of the lattice coupling constant β in the figure. The relevant value of β is indicated near the peaks corresponding to the IR clusters. One can see that the leftmost peaks, corresponding to the UV clusters, are almost indistinguishable in this figure. We also note that for all considered values of β the infrared cluster and the ultraviolet clusters can be unambiguously separated due to a wide gap between them.

A similar picture is observed for blocked monopoles. This can be seen from Fig. 1(b) in which we show typical distributions of $n=2$ blocked monopoles.

According to Figs. 1(a) and 1(b) the gap between IR and UV clusters becomes smaller as the *physical* lattice size decreases. At very small lattice size the gap between UV and IR clusters disappears and the IR and UV clusters cannot be separated. This behavior of the monopole clusters leads to the deconfining transition (''crossover'') which takes place in sufficiently small physical volumes.

The distribution of the ultraviolet clusters was studied both numerically [11,14] and analytically [13,18]. The distribution can be described by a power law $D_{UV} \propto L^{-\tau}$, where the power τ is very close to 3. This behavior indicates that the monopoles in the UV clusters show a random walk picture [13]. In our simulations we mainly concentrate on the IR monopole cluster because, as we have already mentioned in the Introduction, the IR cluster is important for the confinement of quarks.

In general, the monopole action $S_{\rm eff}^{\rm mon}$ could be represented as a sum of n-point ($n \geqslant 2$) operators S_i [4,20]:

$$S[k] = \sum_i f_i S_i[k], \tag{10}$$

where f_i are coupling constants. In this paper we adopt only dominant two-point interactions in the monopole action [i.e. interactions of the form $S_i \sim k_\mu(s) k_{\mu'}(s')$] [19]. Following Ref. [4] we derive the effective monopole action (10) from the configurations of monopole currents, $\{k_\mu(s)\}$ using an inverse Monte Carlo method.[2] The original monopole configurations were generated by the usual heat-bath Monte Carlo algorithm of SU(2) gluodynamics.

The dominant term in the monopole action (10) is the most local self-interaction of the monopole currents, $S_1[k] = \Sigma_{s,\mu} k_\mu^2(s)$. The contributions to the action from other interactions are small compared to the leading term. As an example we show the leading contribution and the full action associated with the IR monopole cluster for $\beta=2.4$ and $n=1,2$ in Fig. 2. Moreover, one can find that both the monopole action and the leading self-coupling contribution to it are proportional with a good accuracy to the length of the monopole loop.

In Fig. 3 we plot the ratio $S[k]/L$ for various lattice volumes and blocking sizes.[3] One can notice that S/L depends almost only on a product $b=a \cdot n$ and does not depend on the variables a and n separately. This was first observed in Ref.

[2]The detailed algorithm is described in Appendix A of Ref. [19].

[3]In this figure and all other figures below we plot all dimensional quantities in units of the string tension, σ.

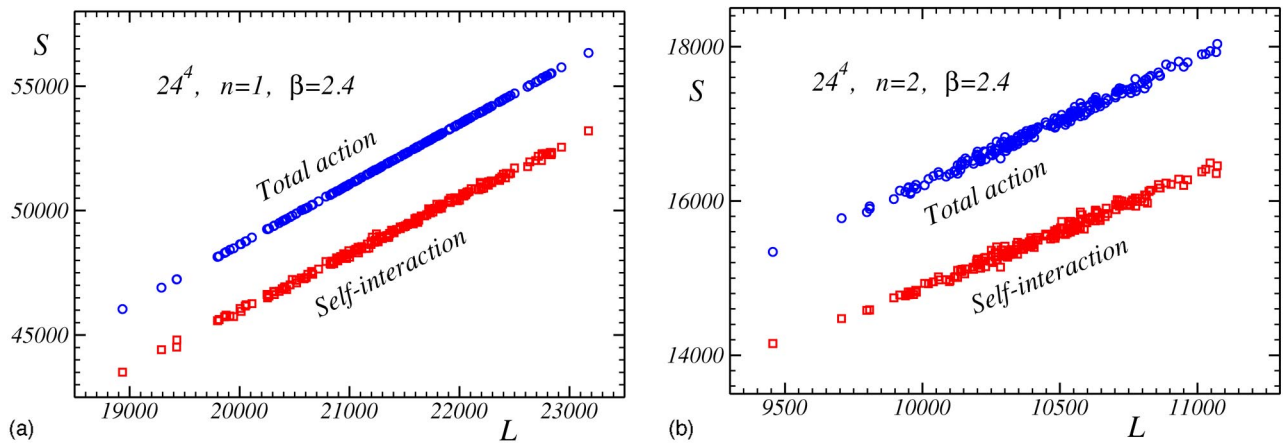

FIG. 2. The total monopole action and the contribution of the self-interaction term to the action for (a) elementary and (b) $n=2$ extended monopoles vs length of the monopole trajectory in the IR cluster as calculated on 24^4 lattice at $\beta=2.4$.

[4]. Below we will observe this type of scaling in many other monopole quantities. Another observation is that the monopoles obtained with the SA procedure have the same action as that of the monopoles defined by the usual iterative gauge-fixing algorithm.

It would also be interesting to compare the monopole action associated with the IR cluster and the action associated with the whole monopole ensemble. The simplest quantity to compare is the f_1 self-coupling parameter which is a dominant coupling in the action. In Fig. 4 we show f_1 for both ensembles. First, we easily notice that the coupling constant f_1 is independent of the lattice volume. Second, we see that for large blocking scales b the type of the ensemble (the IR cluster or the whole ensemble) is not essential for the determination of f_1. However, at small b values, $b\sqrt{\sigma}\lesssim 0.5$, the type of the lattice ensemble becomes important, since in this region

$$f_1^{\mathrm{IR}} > f_1^{\mathrm{total}}, \quad \text{for } b\sqrt{\sigma}\lesssim 0.5. \tag{11}$$

The observed difference between the couplings can be affected by finite-size effects since the leftmost points in our data correspond to elementary (of size a) monopoles. Moreover, in our studies we included only the two-point interactions in the monopole action (10). However, two-point actions alone becomes unreliable at too small values of b and one has to include higher-point interactions [19].

The observation (11) may have a physical meaning related to a simple fact that the larger coupling f_1 corresponds to the smaller density of the monopoles. Thus Eq. (11) is in agreement with the numerical fact that at large lattice coupling β (i.e., at small lattice spacing a) the density of the monopoles in the largest cluster is noticeably smaller than the total monopole density [21].

IV. MONOPOLE LENGTH DISTRIBUTION FOR IR CLUSTER

Since the density of the elementary monopoles from infrared clusters is finite (in terms of physical units) in the continuum limit [21], we may expect that the density of the extended monopoles (with a fixed blocking scale b) is finite as well. The finiteness of the density is consistent with the observation that the monopole length distribution is localized around a certain value of the monopole length $L_{\max}$ (see Fig. 1). As will be shown, this value is proportional to the physical volume V of the system, $L_{max}\propto V$. Indeed, as one can qualitatively find from Fig. 1, the position of the peak of the IR length distribution increases as the physical volume of the

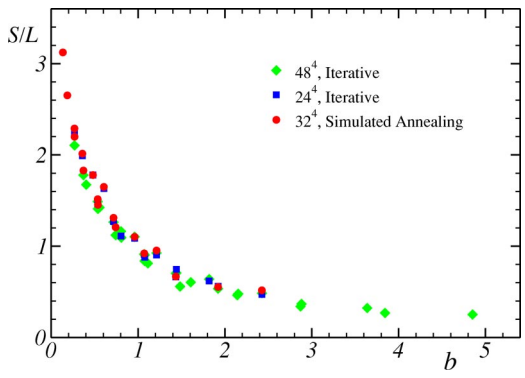

FIG. 3. The ratio S/L, in physical units, as a function of b for various lattices N^4 and blocking steps n.

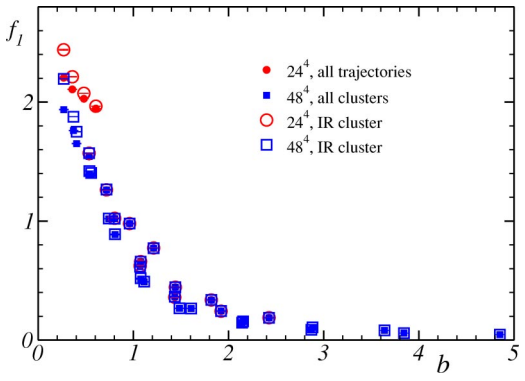

FIG. 4. The self-interaction coupling constant f_1 as the function of b calculated for the largest monopole cluster and for the whole monopole ensemble on lattices 24^4 and 48^4.

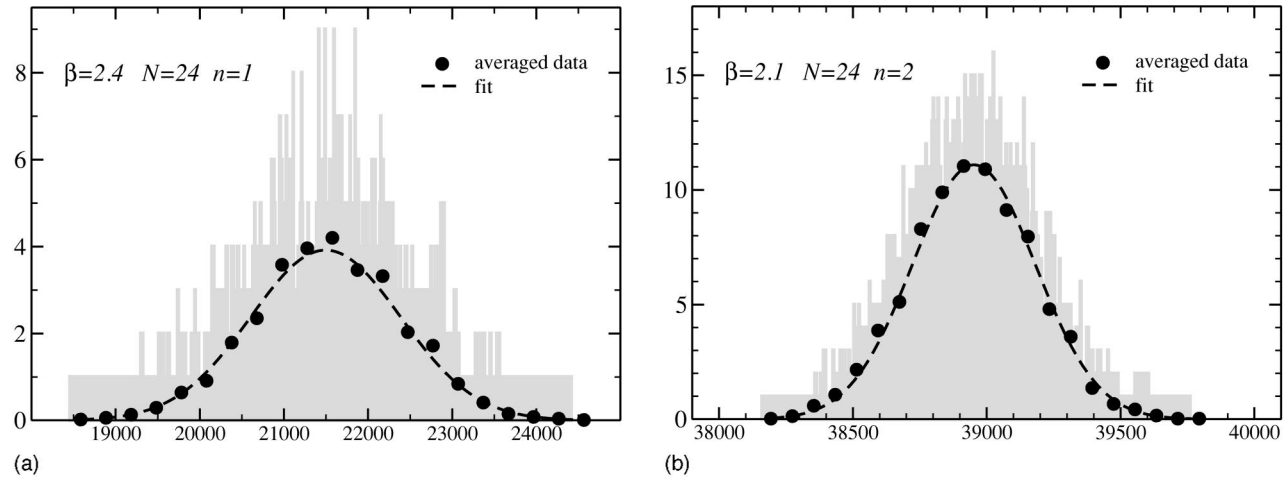

FIG. 5. Illustration of the Gaussian distribution of the IR monopole clusters on 24^4 lattice (a) for elementary monopoles at $\beta=2.4$ and (b) for blocked, $n=2$ monopoles at $\beta=2.1$. The original histograms of the length distribution in the IR cluster are shown by gray shading. The averaged distributions are shown by circles, and the fits by the function (14) are represented by the dashed line.

system. Note that the physical volume of the system decreases as the lattice coupling β becomes larger.

The length distribution function, $D(L)$, is proportional to the weight with which the particular trajectory of the length L contributes to the partition function. On the other hand, the action of a monopole trajectory is proportional to the length of the trajectory, $S\propto L$, as we have illustrated in the previous section. Thus the monopole action contributes to the weight in a form of an exponential factor, $\propto e^{-fL}$. Here f is a parameter which is close to the self-coupling f_1 according to Fig. 4. The entropy of the monopole trajectory also contributes to the monopole length distribution, which is proportional to μ^L (with μ being a positive number) for sufficiently large monopole length L. Thus the distribution of the monopole trajectories in the infinite volume limit must be described by a function

$$D^{IR}_{\rm inf}(L)\propto \mu^L\cdot e^{-fL}=e^{\gamma L},\quad \gamma=\ln\mu-f. \tag{12}$$

In this equation we neglect a power-law prefactor which is essential for the distribution of the ultraviolet clusters[4] [13].

The observed localization of the infrared cluster distribution implies a certain cut which depends on the volume of the system. The simplest distribution of this kind may be described by a function

$$D^{IR}(L)=\exp\{-\alpha L^{\eta}+\gamma L\}, \tag{13}$$

where α, γ and η are certain parameters.

As we find below, the parameter η which characterizes the cut due to the volume effect is $\eta\approx 2$. Moreover, as we mentioned, the parameter γ characterizes the action and the entropy of the monopole currents and thus it must depend only on the physical size of the blocked monopole, $\gamma=\gamma(b)$. On the other hand, α must depend both on the physical size and the volume, i.e., $\alpha=\alpha(b,V)$. Thus we assume the following parametrization of the IR monopole distribution at finite volume:

$$D^{IR}(L)=\exp\{-\alpha(b,V)L^2+\gamma(b)L\}. \tag{14}$$

Then the peak of the distribution (14) becomes

$$L_{max}=\frac{\gamma(b)}{2\alpha(b,V)}. \tag{15}$$

The IR monopole density is given by

$$\rho_{IR}=\frac{L_{max}}{V}=\frac{\gamma(b)}{2\alpha(b,V)V}, \tag{16}$$

in the thermodynamic limit, $V\to\infty$ and is expected to be finite. Hence we see $L_{max}\propto V$. From Eq. (16) we conclude that

$$\alpha(b,V)=A(b)/V, \tag{17}$$

where the function $A(b)$ depends only on the size of the blocked monopole, b. Equation (17) implies that in the thermodynamic limit the parameter α vanishes and the finite-volume distribution (13) is reduced to Eq. (12), as expected.

Let us check the distribution (14) numerically. We show typical examples of the IR cluster distributions in Fig. 5. One can see that these histograms have an almost symmetric structure. But due to the lack of statistics, these histograms cannot be fitted by the function (14). In order to show that the distribution of the lengths of the monopole trajectories follows Eq. (14), we smooth the noise in Fig. 5 by increasing the bin size from the original size of $\delta L=2$ to $\delta L=200$ [for the case presented in Fig. 5(a)] and to $\delta L=70$ [for Fig. 5(b)]. Thus, effectively, we average the data inside each coarser bin and, as a result, we reduce the noise.

[4]Below we work with the distribution of the pure exponential form (12). We also repeated our analysis with the prefactor L^{-3} included. We observed that the results with and without the power-law prefactor are the same within the small error bars.

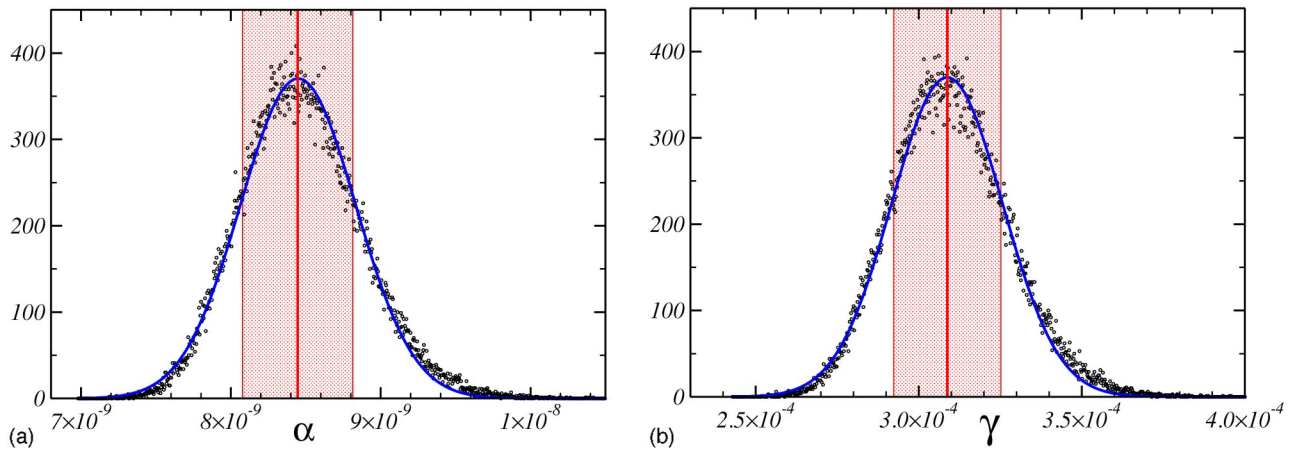

FIG. 6. The distribution of the parameter α and γ for elementary monopoles at $\beta=2.4$ on 24^4 lattice. The fits by a Gaussian function are shown by the solid lines and the value of the errors are indicated by shadowed regions.

The averaged (and suitably rescaled) histograms and their fits by the function (14) are shown in Fig. 5. One can see that the averaged histograms are very close to the Gaussian distribution. Similar behavior can also be observed for all IR monopole cluster distributions we have studied in this paper.

In order to justify the chosen value of the parameter η in Eq. (14) we have also fitted the averaged histogram data by Eq. (13) in which η is treated as a fitting parameter. The best fit (for $\beta=2.4$ and $n=1$ on 24^4 lattice, as an example) gives us the result $\eta=2.05(15)$. Fits of other histograms give us similar results. Thus we fix below $\eta=2$.

The histograms in Fig. 5 were obtained with rather high simulation statistics (3000 configurations according to Table I). However, in order to get a perfect Gaussian, we need much more statistics which require a lot of CPU time. To avoid this lengthy procedure we assume[5] that the numerical data for length distribution of the IR monopoles are described by Eq. (14). Then one can evaluate the central values of the parameters α and γ using simple formulas (valid for a Gaussian distribution),

$$\alpha=\frac{1}{2}\frac{1}{\langle L^2\rangle-\langle L\rangle^2},\qquad \gamma=\frac{\langle L\rangle}{\langle L^2\rangle-\langle L\rangle^2},\tag{18}$$

where the averaging $\langle\cdots\rangle$ is performed using weights from the histograms.

To evaluate the errors for the parameters α and γ, we use the standard bootstrap method. Namely, we make a resampling of the original length distribution of the IR monopole clusters, $L_{\max}$. We construct a resampled distribution by selecting n_{conf} random values of $L_{\max}$ where n_{conf} is the total number of the monopole configurations. Note that any element of the original distribution may enter the resampled distribution more than one time.

After the resampled configuration is constructed we evaluate the values of the parameters α and γ on this configuration using Eq. (18). We generate a number of such configurations and then construct the distributions of the parameters α and γ. These distributions are the Gaussian functions with the widths equal to the corresponding errors. We plot examples of the histograms for α and γ values in Figs. 6(a) and 6(b).

We have checked the applicability of Eqs. (18) and the use of the bootstrap method on a smaller, 16^4, lattice. Namely, we have generated length distributions using from low statistics (2000 configurations) to high statistics (10^5 configurations) ensembles. We used the bootstrap method along with Eqs. (18) to evaluate the coefficients α and β for the distribution measured with the lowest statistics. On the other hand, the high statistics distribution is a (almost perfect) Gaussian and therefore we get the desired coefficients directly from the fit (14). The comparison of the coefficients shows that the central values as well as the estimated errors for the low and for the high statistics ensembles coincide with each other within a few percent. We illustrate our analysis in Fig. 7 for $\beta=2.1$ and $\beta=2.2$ using the parameter γ as an example. The values of γ obtained with the standard method are plotted vs number of configurations, N_{conf}, used in the analysis. The horizontal lines represent the results coming from the bootstrap method applied to the low-

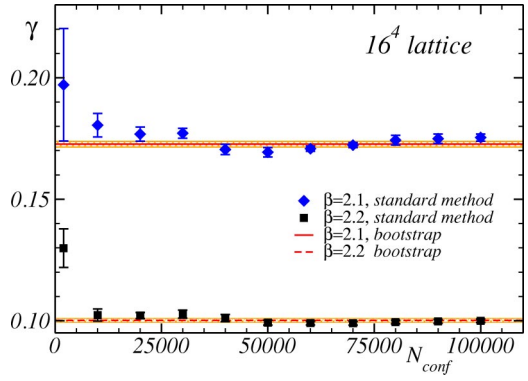

FIG. 7. Check of the bootstrap method on 16^4 lattice illustration with parameter γ (the explanation is given in the text).

[5]We are checking this assumption on a smaller lattice at the end of this section.

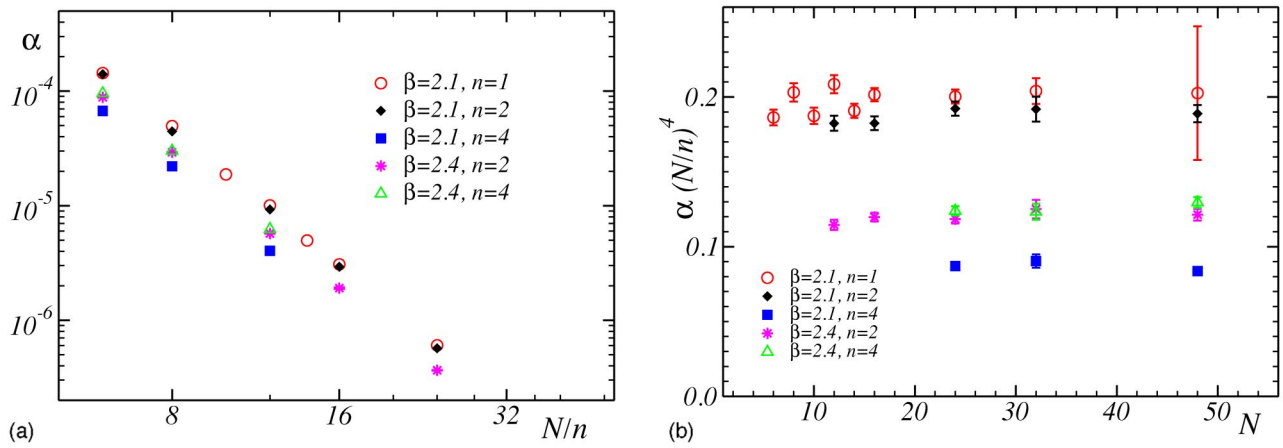

FIG. 8. (a) The fitting parameter α as a function of the size N/n of the coarse lattice; (b) the parameter α multiplied by the lattice volume as a function of the lattice size N.

statistic ensemble (the statistical errors are indicated by shadowed regions). We conclude that the bootstrap method gives reliable results using the distributions with low statistics.

In order to confirm our expectation (17) we plot the parameter α vs the ratio N/n in Fig. 8(a) for selected sets of coupling constants β and the blocking steps of the monopole, n. Since the volume of the blocked lattice is $(N/n)^4$, we expect that the parameter α behaves as $\alpha \propto (N/n)^{-4}$. This behavior is seen in Figs. 8(a) and 8(b). The parameter α multiplied by the lattice volume is almost independent of the lattice size N according to Fig. 8(b).

According to our discussion above, the fitting parameter γ must be a function of the blocking size b alone and does not depend on the volume of the lattice. In Fig. 9 we show the parameter γ is indeed independent of the lattice size N.

The fitting parameters α and γ are shown as functions of the physical scale b in Figs. 10(a) and 10(b), respectively. The parameter γ shows the scaling behavior in a sense that it depends on the blocking step n and lattice spacing a only in the form of the product $b=n\cdot a$.

V. MONOPOLE DENSITY AND ENTROPY

A. Monopole density

The simplest physical observable of the monopole ensemble is its density. It is interesting to compare the monopole density obtained from the IR monopole cluster distribution, Eq. (16), with the direct observation of the monopole density,

$$\rho_{IR}=\frac{1}{4(na)^3\cdot(N/n)^4}\left\langle \sum_{s,\mu} |k_\mu^{(n)}(s)| \right\rangle. \qquad (19)$$

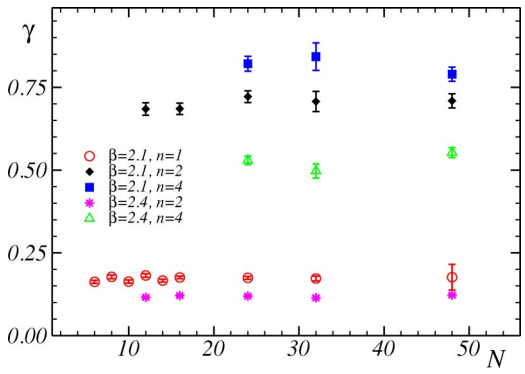

FIG. 9. The illustration of the independence of the fitting parameter γ on the lattice size, N.

Here the blocked monopole current $k_\mu^{(n)}$ is defined by Eq. (6). The normalization factor in Eq. (19) appears naturally if one notes that $b=na$ and $4(N/n)^4$ are the lattice spacing and the number of links of the coarse lattice, respectively.

If the fitting function (14) describes the data correctly, one should observe the same infrared monopole density obtained from the fits of the monopole distributions (14), (16) as that obtained in a direct way (19). This is indeed the case according to Fig. 11(a).

We note that the value of the blocked monopole density quoted above is about 30% larger than the value of density [21] of the *elementary* infrared monopoles in the continuum limit.

The monopole density is known to be sensitive to the details of the gauge fixing procedure [21]. In order to check the effect of the gauge fixing we compare in Fig. 11(b) the infrared monopole density obtained using the SA and iterative gauge fixing algorithms. One can see from this figure that at large b there is practically no difference between the monopole densities obtained with the use of the different algorithms. However, there exists some difference at small b since the SA monopole density is smaller than the density obtained with the help of the iterative algorithm. This slight dependence of the density on the gauge fixing algorithm at small b may explain the discrepancy between our results and the results of Ref. [21] mentioned above. Another source of the discrepancy is the qualitative difference between the elementary and the blocked monopoles. Since the scale b is taken to be independent of the lattice spacing a while a tends to zero in the continuum limit, the elementary monopoles are expected to be more affected by the ultraviolet lattice artifacts.

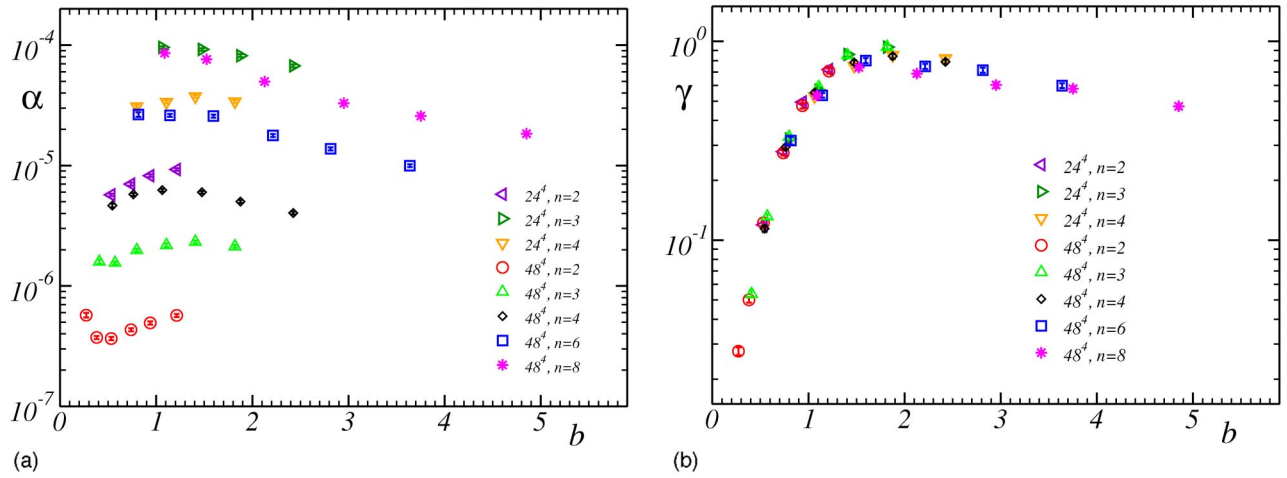

FIG. 10. The fitting parameters (a) α and (b) γ as a function of b for various lattice volumes N^4 and monopole blocking steps n.

B. Monopole entropy

The distribution of the monopole trajectories depends both on the monopole action and on the monopole entropy as we have already discussed in Sec. IV. Therefore the knowledge of the distribution and the monopole action allows us to extract the entropy of the monopole currents. If the monopoles make a simple random walk on the four-dimensional hypercubic lattice, the entropy factor for elementary monopoles is expected to be equal to seven, $\mu=7$, since there are seven choices at each site for the monopole current to go further (the monopole trajectory is obviously nonbacktracking due to the presence of the magnetic charge).

The entropy factor μ of the infrared monopole trajectories can be obtained from the IR cluster distribution and the monopole action according to Eq. (12),

$$\mu = e^{\gamma+f}. \tag{20}$$

We calculate numerically the parameters γ and f to find the entropy factor μ for various scales b and lattice sizes. Our results are presented in Fig. 12. The entropy shows an approximate scaling behavior in a sense that the entropy depends only on the scale b and is independent of the lattice spacing a and the blocking factor n separately. One can also notice that the entropy μ is independent of the volume of the lattice. The largest scaling violation happens at small blocking sizes $n=1,2$ where the finite-size artifacts are expected to be strong.

The entropy factor μ is a descending function of the scale b. As discussed above, one can expect that the factor μ should be equal to seven for elementary monopoles. However, we see $\mu>7$ for small values of b from Fig. 12. We explain this small-b behavior as an artifact of our numerical procedure adopted in this paper. Indeed, we used the quadratic monopole action. However, at small b, higher-point interaction terms are essential and thus the monopole action cannot be reliably described by the quadratic terms only [19,20].

At large b the entropy factor (20) is smaller than seven. Formally this means that the motion of the blocked monopoles is constrained. We have fitted the entropy by a function

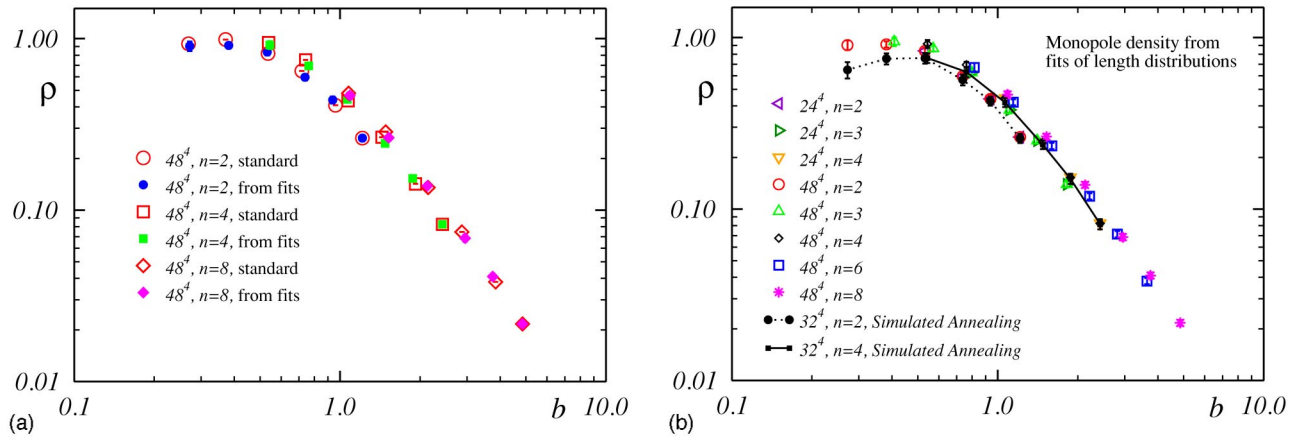

FIG. 11. (a) Comparison of the infrared monopole density obtained from the fits of the monopole distributions (14), (16) with the density obtained in a direct way (19). (b) Comparison of the effect of the gauge fixing procedure (iterative vs simulated annealing) on the infrared monopole density.

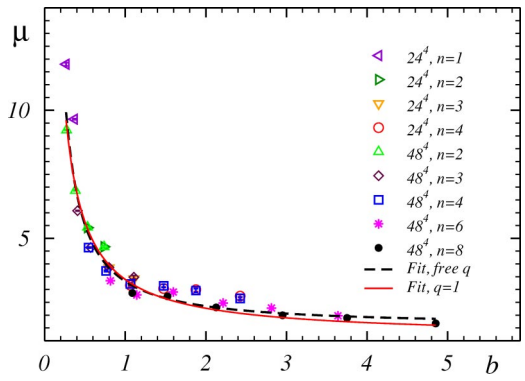

FIG. 12. Entropy factor μ vs b. The dashed line represents the fit by Eq. (21) with free q parameter and the solid line corresponds to the fixed parameter, $q=1$.

$$\mu^{\mathrm{fit}}=\mu_\infty+C\mu^{-q}, \tag{21}$$

where μ_∞, C and q are fitting parameters. The best fit is shown in Fig. 12 by the dashed line. The corresponding best fit parameters are $\mu_\infty=1.6(4)$, $C=1.7(5)$ and $q=1.2(2)$. The most interesting fitting parameter is μ_∞ which is the asymptotic value of the entropy in the infrared limit $b\sigma^{1/2}\to\infty$ according to Eq. (21). Unfortunately, the value of the asymptotic entropy is obtained with a big error bar in the above fit. In order to increase the accuracy we notice that the power q is very close to unity. Fixing $q=1$ in Eq. (21) and repeating the fitting procedure again, we get $\mu_\infty=1.15(25)$ and $C=2.2(1)$. The corresponding best fit curve is shown in Fig. 12 by the solid line.

The fact that the asymptotic value of the entropy is very close to unity in the limit $b\sigma^{1/2}\to\infty$ may have a simple explanation. The monopole with a large blocking size b behaves as a classical object and its motion is never a simple random walk. The predominant motion of the large-b monopole is close to a straight line.

VI. CONCLUSION

We studied numerically the distributions of the infrared monopole currents of various blocking sizes n on the lattices with different spacings a and volumes N. The distributions can be described by a Gaussian ansatz with a good accuracy. The ansatz contains two important terms: (i) the linear term which has information about the energy and the entropy of the monopole currents; and (ii) the quadratic term which suppresses too large infrared clusters. The linear term is independent of the lattice volume while the quadratic term is inversely proportional to the volume. The monopole density determined from the parameters of the Gaussian fits coincides with the result of the direct numerical calculation.

We also studied the action of the monopoles belonging to the infrared clusters and compared it with the action of the total monopole ensemble. It turns out that the self-coupling coefficients for both these ensembles are almost the same at large b. However, as the blocking scale b is decreased the self-coupling coefficient for an infrared monopole cluster gets noticeably larger than the coefficient for the total monopole ensemble. This can be explained by the fact that the self-interaction coefficient is related directly to the monopole density.

The knowledge of both the coefficient in front of the linear term of the Gaussian distribution and the monopole action for infrared clusters allows us to determine the entropy factor of the extended (blocked) monopole currents. We have numerically shown that the entropy of the blocked monopole currents is a descending function of $b=na$, indicating that the effective degrees of freedom of the blocked monopoles are getting smaller as the physical classical picture: the monopole becomes a macroscopic object and the motion of such a monopole is close to a straight line.

ACKNOWLEDGMENT

M.Ch. acknowledges the support by JSPS grant No. P01023. T.S. is partially supported by a JSPS Grant-in-Aid for Scientific Research on Priority Areas No. 13135210 and (B) No. 15340073.

[1] G. 't Hooft, in *High Energy Physics*, edited by A. Zichichi, EPS International Conference, Palermo (1975); S. Mandelstam, Phys. Rep. **23**, 245 (1976).
[2] G. 't Hooft, Nucl. Phys. **B190**, 455 (1981).
[3] T. Suzuki, Nucl. Phys. B (Proc. Suppl.) **30**, 176 (1993); M. N. Chernodub and M. I. Polikarpov, in *Confinement, duality, and nonperturbative aspects of QCD*, edited by P. van Baal (Plenum Press, New York, 1998), p. 387; R.W. Haymaker, Phys. Rep. **315**, 153 (1999).
[4] H. Shiba and T. Suzuki, Phys. Lett. B **351**, 519 (1995).
[5] N. Arasaki, S. Ejiri, S.i. Kitahara, Y. Matsubara, and T. Suzuki, Phys. Lett. B **395**, 275 (1997); M.N. Chernodub, M.I. Polikarpov, and A.I. Veselov, *ibid.* **399**, 267 (1997); Nucl. Phys. B (Proc. Suppl.) **49**, 307 (1996); A. Di Giacomo and G. Paffuti, Phys. Rev. D **56**, 6816 (1997).
[6] H. Shiba and T. Suzuki, Phys. Lett. B **333**, 461 (1994).
[7] T. Suzuki and I. Yotsuyanagi, Phys. Rev. D **42**, 4257 (1990); G.S. Bali, V. Bornyakov, M. Müller-Preussker, and K. Schilling, *ibid.* **54**, 2863 (1996).
[8] Y. Koma, M. Koma, E.M. Ilgenfritz, T. Suzuki, and M.I. Polikarpov, Phys. Rev. D **68**, 094018 (2003).
[9] T.L. Ivanenko, A.V. Pochinsky, and M.I. Polikarpov, Phys. Lett. B **252**, 631 (1990).
[10] S. Kitahara, Y. Matsubara, and T. Suzuki, Prog. Theor. Phys. **93**, 1 (1995).
[11] A. Hart and M. Teper, Phys. Rev. D **58**, 014504 (1998).
[12] P.Y. Boyko, M.I. Polikarpov, and V.I. Zakharov, Nucl. Phys. B (Proc. Suppl.) **119**, 724 (2003).
[13] M.N. Chernodub and V.I. Zakharov, Nucl. Phys. **B669**, 233 (2003).
[14] V.G. Bornyakov, P.Yu. Boyko, M.I. Polikarpov, and V.I. Zakharov, Nucl. Phys. **B672**, 222 (2003).

[15] A.S. Kronfeld, M.L. Laursen, G. Schierholz, and U.J. Wiese, Phys. Lett. B **198**, 516 (1987); A.S. Kronfeld, G. Schierholz, and U.J. Wiese, Nucl. Phys. **B293**, 461 (1987).
[16] T.A. DeGrand and D. Toussaint, Phys. Rev. D **22**, 2478 (1980).
[17] G.S. Bali, V. Bornyakov, M. Muller-Preussker, and K. Schilling, Phys. Rev. D **54**, 2863 (1996).
[18] V.I. Zakharov, "*Hidden Mass Hierarchy in QCD*," hep-ph/0202040.
[19] S. Kato, S. Kitahara, N. Nakamura, and T. Suzuki, Nucl. Phys. **B520**, 323 (1998).
[20] M.N. Chernodub, S. Fujimoto, S. Kato, M. Murata, M.I. Polikarpov, and T. Suzuki, Phys. Rev. D **62**, 094506 (2000); M.N. Chernodub, S. Kato, N. Nakamura, M.I. Polikarpov, and T. Suzuki, "*Various representations of infrared effective lattice SU(2) gluodynamics*," hep-lat/9902013.
[21] V. Bornyakov and M. Muller-Preussker, Nucl. Phys. B (Proc. Suppl.) **106**, 646 (2002).
[22] T. Banks, R. Myerson, and J.B. Kogut, Nucl. Phys. **B129**, 493 (1977).
[23] H. Shiba and T. Suzuki, Phys. Lett. B **343**, 315 (1995).